

# Dynamics of Heatwave Intensification over the Indian Region

Lekshmi S<sup>1,2</sup>, Rajib Chattopadhyay<sup>1,4</sup>, D.S. Pai<sup>3</sup>

<sup>1</sup> India Meteorological Department, Pune

<sup>2</sup> Savitribai Phule Pune University, Pune

<sup>3</sup> India Meteorological Department, New Delhi

<sup>4</sup> Indian Institute of Tropical Meteorology, Pune

Corresponding Author:

**Rajib Chattopadhyay**

**Email:** [rajib@tropmet.res.in](mailto:rajib@tropmet.res.in)

**ORCID Id:** <https://orcid.org/0000-0002-1973-7307>

## **Abstract**

In a warming world, heatwaves over India have become intense and are causing severe health impacts. Studies have identified the presence of amplified Rossby waves and their association with the intensification of heatwaves. Earlier studies have identified two dominant modes of temperature variability in India and their possible role in the development of dry (mode-1) and moist (mode-2) heatwaves. These modes are associated with midlatitude Rossby waves intruding over the Indian region. However, the role of regional forcing and the teleconnection behind the intensification of the heatwaves over India is missing. The present study has analyzed the dynamical mechanisms for the regional intensification of the circulation features associated with the dominant moist heatwave mode (mode-2).

Considering the predominant barotropic nature of the observed circulation features of the mode, a simple barotropic vorticity equation model forced with extratropical and regional vorticity sources is used to understand the intensification of the heat waves. It was found that a wave response initiated by a cyclonic vorticity over the Bay of Bengal superimposes with the mid-latitude anticyclonic vorticity generated Rossby waves intruding over India. This superimposition results in the amplification and persistence of the anticyclonic vorticity phase over the Northwest Indian region, leading to the intensification of circulation. It was also found that the barotropically forced intensified circulation leads to the intensification of the heat stress. Under a climate change scenario, different '*circulation regimes*', characterized by zonal stationary wave number and jet speed, which can favor the intensification are also identified.

## 1. Introduction

Over the Indian region, intense heatwaves and heat stress are significant environmental hazards that have severe impacts in different sectors. Increased exposure to excess heat can have adverse effects on health and, together with humidity, can cause heat strain and discomfort, leading to heat injury (Sharma et al. 1983; Taylor et al. 2008). The driving mechanism of the intensification of heatwaves is influenced by multi-scale spatiotemporal processes. This comprises large-scale climate variability and teleconnection patterns such as ENSO (Kenyon and Hegerl 2008), synoptic scale features such as Rossby wave activity or blocking highs (Matsueda 2011; Meehl and Tebaldi 2004), and local factors such as land use land cover and soil moisture conditions (Alexander 2011). Over the Indian region, studies have pointed towards the possible role of mid-latitude Rossby waves (Rohini et al. 2016; Ratnam et al. 2016), impact of Indian Ocean (Roxy et al. 2015), climate drivers such as El-Nino (Murari et al. 2016; PAI and NAIR 2022) and depleted soil moisture (Ganeshi et al. 2020, 2023) in driving the heat extremes. The observed trends (Perkins et al. 2012; Perkins-Kirkpatrick and Lewis 2020) as well as projections (IPCC 2013, 2021) show an increase in the intensity, frequency and duration of heatwaves both globally and regionally. Such a rise in intensity and frequency of heatwaves is observed over the Indian region (Pai et al. 2013, 2017; Rohini et al. 2016) which is also evident from the heat-related mortality rate (Guleria and Gupta 2016; Mazdiyasnani et al. 2017).

Previous studies have identified that the extratropical Rossby wave intrusion over the Indian region can cause significant modulations in weather features, such as extremes (Kalshetti et al. 2022; White et al. 2022). Different teleconnection pathways can link the Rossby wave source regions to remote locations (Simmons et al. 1983). The propagation of Rossby waves through subtropical westerly jetstream which can act as a waveguide, is one such pathway (Teng and Branstator 2019). Lekshmi and Chattopadhyay 2022 (hereafter referred to as LC22) has identified two dominant modes associated with such teleconnection pathways that cause summer temperature intraseasonal variability over the Indian region. Based on the regional impact caused, these modes were further attributed as the dry and moist heat stress modes in Lekshmi et al., 2024. These waves are known to cause intraseasonal variabilities in temperature that sometimes leads to extreme events. Then, what differentiates an intensified heatwave with a normal one? Or, from wave propagation perspective, what differentiates the waves from causing ‘normal’ (climatology) to ‘anomalous’ fluctuations (extremes)? One of the primary synoptic-scale feature associated with every heatwave is the

upper-air anticyclonic circulations, which are often caused by the blocking highs (Matsueda 2011; Perkins 2015) or the stationary/propagating Rossby waves (Kornhuber et al. 2020; Parker et al. 2014). Such systems can cause ‘normal’ fluctuations and sometimes extremes such as heatwaves. The two possible reasons for such ‘anomalous’ fluctuations are (i) amplification of the circulation or (ii) its persistence over the region for a longer duration.

Amplification of circulation features can occur as a result of many factors such as (a) *High amplitude quasi-stationary Rossby waves* (b) *Quasi-resonant amplification (QRA)* or (c) *Superimposing waves*. With the amplified Rossby waves 5 and 7, there has been an increase in the occurrence of concurrent heat extremes in different regions in America, Europe and Asia (Kornhuber et al. 2019, 2020; Coumou et al. 2014). Such ‘phase-locking’ of hemispheric patterns are favored by local topography (Jiménez-Esteve et al. 2022; Jiménez-Esteve and Domeisen 2022). Latitudinal trapping and amplification of quasi-stationary free synoptic-scale Rossby waves can occur through the quasi-resonance of free and forced waves in the midlatitude waveguides (Petoukhov et al. 2013; Kornhuber et al. 2017) which can lead to heatwaves (Rao et al. 2021). It has been shown that the response to winter-time El-Nino convective forcing over tropical Pacific is due to the combined effect of westward propagating and eastward propagating barotropic Rossby waves (Shaman and Tziperman 2016). This leads to a predominantly linear superposition of these oppositely directed waves which are trapped inside the North African-Asian jet with weaker nonlinear effects. Such type of linear superposition of waves with the same phase over a region can cause wave amplification, which could further lead to extremes.

Often, the persistence of upper-air anticyclonic circulation over any region for a long time can intensify heatwaves due to the positive feedback during dry conditions (Seneviratne et al. 2006). Absence of any atmospheric processes such as moist air intrusion, convective activity or appearance of another system that shifts the location of anticyclone etc. can cause such systems to linger around. The possible reasons for the highs to persist over a region for a longer time are: (a) formation of stationary/quasi-stationary waves: formation of a thermally/orographically induced stationary/quasi-stationary waves are one such example which, can cause heat extremes (Wolf et al. 2018). Also, studies have shown that quasi-stationary waves with wave numbers 5-7 can lead to humid heat extremes in Northern Hemisphere midlatitudes (Lin and Yuan 2022). (b) slowing down of propagating waves in a weakened jet stream waveguide: This factor is closely related to the climate change and the long-term trend in observed zonal mean wind and jet streams. Recent studies have brought out the role of

weakening of the westerly jet due to weakening meridional thermal gradient (Coumou et al. 2014; Francis and Vavrus 2012). Such a weakening in the zonal mean wind can trigger more waviness in the jet and lead to more mid-latitude extreme weather (Moon et al. 2022). Apart from all these factors, the long-term trends in the mean surface temperatures can cause a shift in the mean temperature. Studies have shown that a small positive shift in the average temperature can cause a disproportionate increase in the intensity and the frequency of extremes (Mearns et al. 1984; Boer and Lambert 2001). But, the shift in the mean alone cannot fully explain the observed magnitude of recent extremes in the Northern Hemisphere mid-latitudes (Petoukhov et al. 2013).

As described in the previous paragraphs, over the Indian region although possible factors for heatwaves are identified, the role of teleconnection pathways and regional factors are not studied well for heatwave intensifications. Thus, there is a need to understand the intrinsic dynamical mechanism that can cause the amplification of heatwaves and in the context of an increase in summer temperature in a warming scenario. Based on the earlier studies, we hypothesize that Rossby wave intrusion and amplification over the Indian region can cause intense heatwaves. Intensification can be studied based on the modes identified by LC22. For mode 1 identified in LC22, the subtropical Rossby wave propagates through the subtropical westerly jet waveguide and reaches over the Indian region. At the same time, for the second mode, the extratropical Rossby waves propagate through the European-Middle East-Indian Ocean pathway (Ambrizzi and Hoskins 1997). Since the intensification of Rossby wave modes has been identified as the driver for heatwave intensification over the Indian region (Fig 8 of LC22), the current analysis will study the relationship of heatwave amplification with teleconnection pathway and regional forcing for mode 2 which shows an increasing trend over the Indian region.

In the climate change scenario, along with the rise in temperature over the Indian region and regional changes in moisture supply (Roxy et al. 2015), notable changes are also occurring in many factors such as stationary wave pattern, zonal wind, jet speed, wave and waveguides, etc. Especially the relationship between jets and the amplification of waves has been debated in the warming scenario (White et al. 2022). While some studies say that weaker jets lead to stronger waves (Francis and Vavrus 2012), other studies propose that weaker jets lead to weaker amplitudes of mid-latitude waves (Manola et al. 2013). Such a wide range of scenarios may impact heatwave intensification. For example, the observed long-term trend in the modes is seen using the time series of their principal components as in

**Fig 1.** While the first mode has a significant decreasing trend, the second mode is having a significant increasing trend. In the present scenario, where climate models are projecting a rise in the heatwave intensity, duration, and frequency over the Indian region (Dubey and Kumar 2023; Goyal et al. 2023), the increasing trend in mode 2 is significant and needs further understanding.

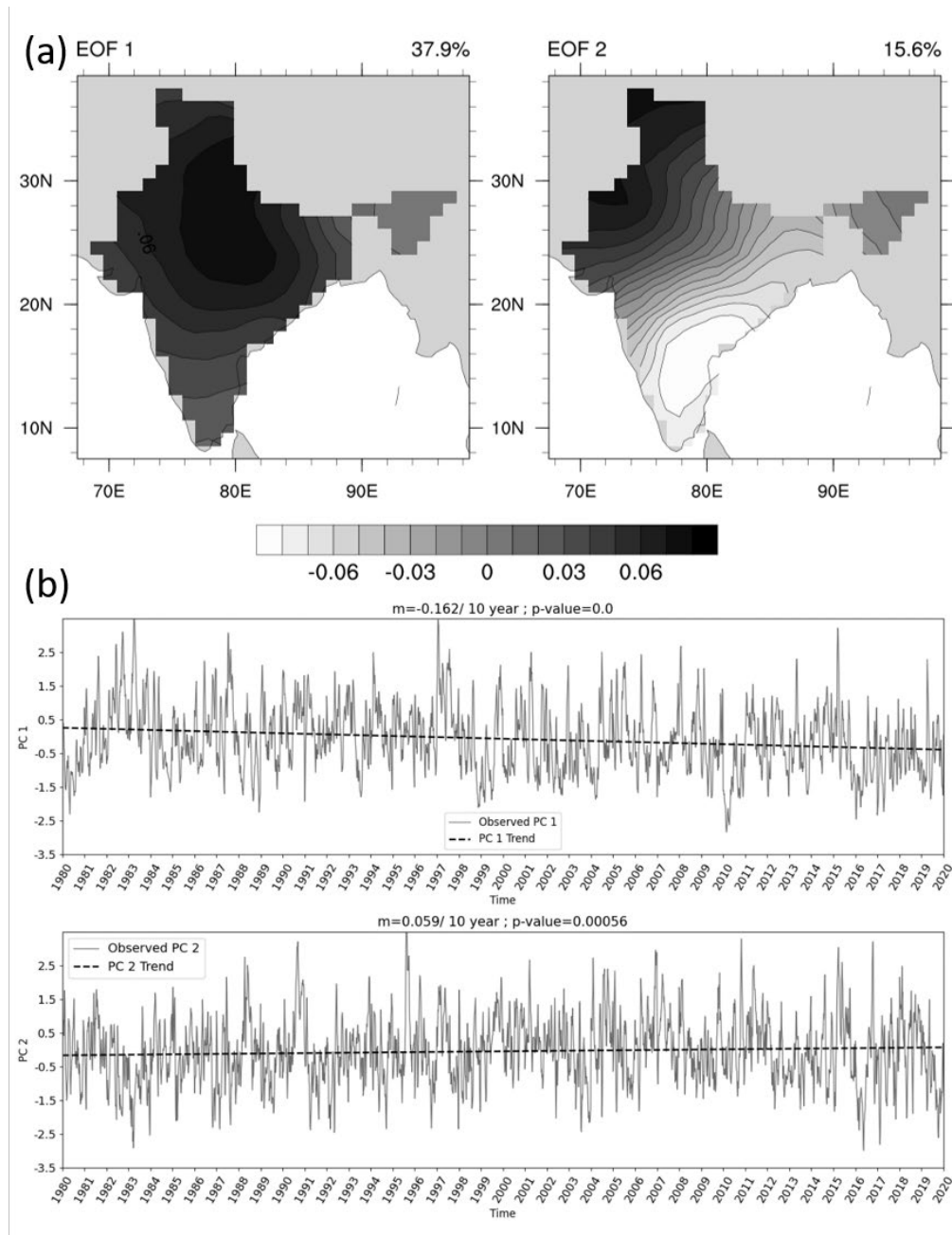


**Figure 1:**(a) Spatial pattern of EOF mode 1 and mode 2 of the April-May detrended surface mean temperature obtained for a period from 1951-2020 (b) Time series of the principal components (PCs) obtained by projecting temperature onto EOF modes from 1980-2020 and their long-term trend

For understanding the formation, propagation, and intensification of Rossby waves in response to thermal or orographic forcing, studies have relied on non-divergent barotropic vorticity equation for a long time (Hoskins and Karoly 1981; Karoly 1983; Hoskins and Ambrizzi 1993; Grimm and Dias 1995). Based on the ratio of barotropic to baroclinic vorticity defined as  $|(\zeta_{850} + \zeta_{200}) / (\zeta_{850} - \zeta_{200})|$ , it is found that over most of the Indian region and over the midlatitudes, the barotropic mode is dominant compared to the baroclinic mode during the days of active mode 2 (Figure not shown). The vertical profile of vorticity over the Northwest Indian region where heatwave occurs confirms this observation (Fig 2a to be discussed later). Hence, in this study, we use the non-divergent barotropic vorticity equation as a toy model to understand the dynamical mechanism associated with mode 2 teleconnection pathways and its intensification over the Indian region.

We believe this analysis will throw some light on the possible processes that cause occasional amplification of the modes of subseasonal variability leading to the intensification of heatwaves and some insights into the same in the context of climate change.

## 2. Data and Methods

The observational patterns associated with mode 2 and its intensification are analyzed using different meteorological parameters. The maximum and minimum temperatures are obtained from India Meteorological Department gridded data of  $1^\circ \times 1^\circ$  resolution (Srivastava et al. 2009). The daily mean temperature is obtained as the mean of maximum and minimum temperature data. For the analysis, the maximum temperature and daily mean temperature data are used. Apart from that, the NOAA Daily Optimum Interpolation Sea Surface Temperature (OI SST) V2 (Huang et al. 2021) of spatial resolution  $0.25^\circ \times 0.25^\circ$  is used for understanding the possible role of regional forcing in mode 2 amplification. Also, the dynamical features associated with mode 2 are analyzed based on the upper level (200 hPa) vorticity pattern and the vertically integrated (1000-300 hPa) moisture flux over the Indian region obtained from the zonal and meridional winds, specific humidity, and mean sea level pressure variables obtained from NCEP DOE Reanalysis 2 dataset which is of  $2.5^\circ \times 2.5^\circ$  resolution (Kanamitsu et al. 2002). The heat stress is assessed based on the NOAA National Weather Service (NWS) Heat Index (<https://www.weather.gov/safety/heat-index>) which is obtained from air temperature and relative humidity (RH) using the inbuilt-function in NCAR Command Language (NCL). The air temperature and RH data for calculating Heat Index (HI) are obtained from the NCEP DOE Reanalysis 2 dataset. All the observational analysis has

been carried out for the period from 1980-2020 for the months of April-May, which are the months when more frequent intense heatwaves occur over India.

### 3. Model Experiments

As mentioned earlier, the dynamical mechanism by which the mode 2 associated Rossby wave is driven and propagates towards the Indian region is looked into using a simple barotropic model framework and an empirical model relating the barotropic model variable output to the other climate parameters. The whole model framework has (i) A *dynamical model* in which vorticity forcing and their response over the Indian region, especially in the intensification of anticyclonic vorticity is considered using the barotropic vorticity equation with prescribed initial conditions. (ii) A simple *Linear Regression model* using which the barotropic model response is evaluated for the temperature. The whole model is set up in such a way as to give a complete framework, beginning from understanding the propagation of mode 2-related anticyclonic circulation and its persistence over the Indian region to the intensification of circulation and finally, its impact in the regional heat stress. Such a hybrid dynamical-statistical modeling framework makes it possible to evaluate the temperature field and further heat stress without explicitly considering the baroclinicity in the dynamical model. The dynamical model here takes the zonal and meridional wind as the input and calculates its non-divergent component. The atmospheric flow evolves based on the barotropic vorticity equation from the input vorticity. The barotropic vorticity equation, given in **Eq 1**, is integrated using a prescribed set of initial conditions (ICs) such as the mean zonal ( $\bar{u}$ ) and meridional ( $\bar{v}$ ) wind, vorticity perturbations ( $\zeta'$  from which  $u'$  and  $v'$  are obtained) with preferred stationary wave pattern ( $z$ ) and any additional vorticity forcing (**Fig 2b**). For all the experiments  $\bar{v} = 0$  (which is not shown in **Fig 2b**).

$$\frac{\partial \zeta}{\partial t} = -J(\psi, f + \zeta) = -\beta v - J(\psi, \zeta) = -\frac{2\Omega}{a^2} \frac{\partial \psi}{\partial \lambda} - J(\psi, \zeta) \quad \text{--- (1)}$$

where  $f = 2\Omega \sin \theta$ ,  $\beta = \frac{2\Omega \cos \theta}{a}$  is the meridional gradient of  $f$  and Jacobian,  $J$  is defined as

$$J(A, B) = \frac{1}{a^2 \cos \theta} \left( \frac{\partial A}{\partial \lambda} \frac{\partial B}{\partial \theta} - \frac{\partial B}{\partial \lambda} \frac{\partial A}{\partial \theta} \right)$$

Where  $a$ ,  $\psi$ ,  $\zeta$ ,  $\Omega$ ,  $\theta$  and  $\lambda$  are radius of Earth, stream function, relative vorticity, angular velocity, latitude and longitude.

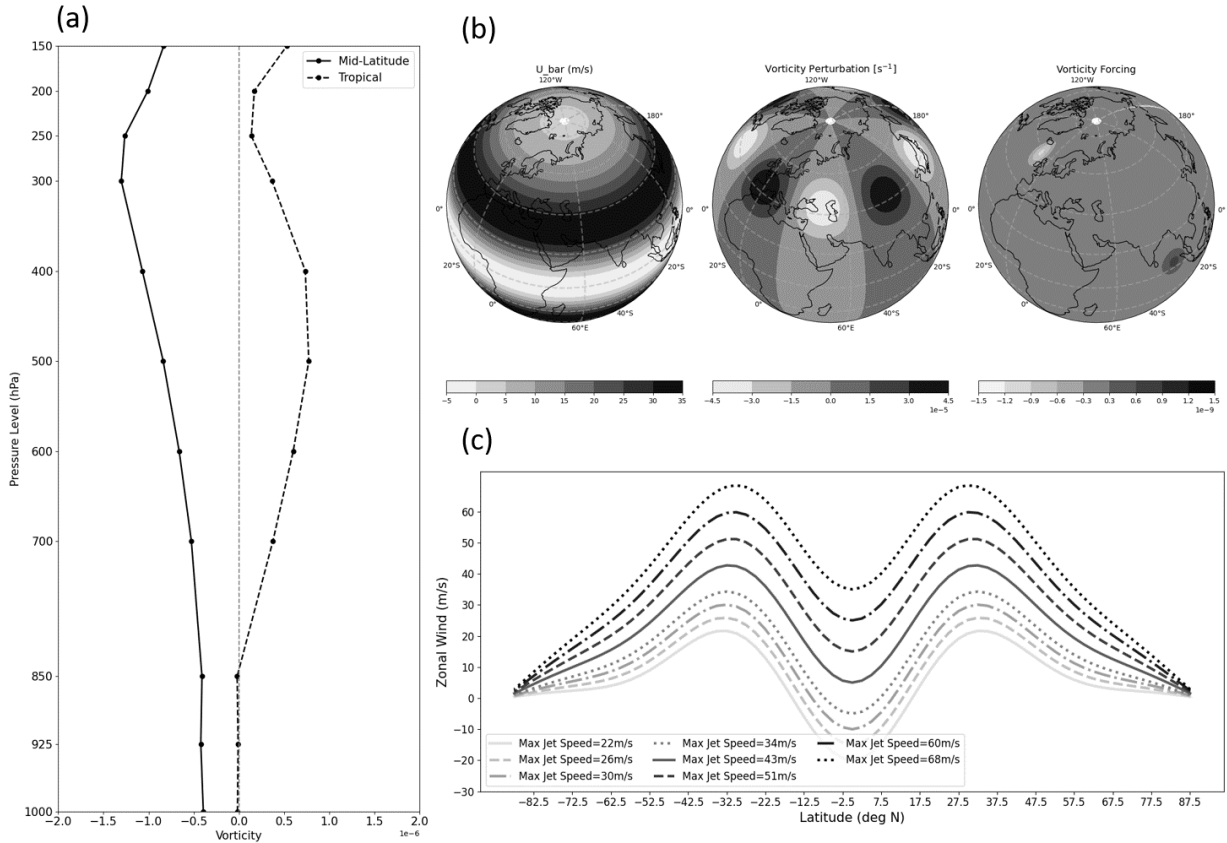


**Figure 2:**(a) Vertical profile of the relative vorticity anomaly composite for those days when  $PC\ 2 > 1.0$  for two regions, one in midlatitude ( $25\text{-}5^\circ\text{W}$ ;  $50\text{-}70^\circ\text{N}$ ) and one in tropics ( $0\text{-}20^\circ\text{N}$ ;  $80\text{-}95^\circ\text{E}$ ) (b)Set of background IC conditions zonal mean wind ( $\bar{u}$ ), vorticity perturbation ( $\zeta'$ ) and vorticity forcing applied for running the barotropic model for  $C(4,34)$  Experiment (c)

Different set of zonally symmetric  $\bar{u}$  used for sensitivity experiments.

Four sets of experiments are designed: (a) *Control Experiment C(4,34)*, where the mode 2 related Rossby wave is generated by placing a mid-latitude vorticity forcing with  $z=4$  and  $j_{max}=34\text{m/s}$ . (b) *Sensitivity Experiment S(4,34)*, where the mode 2 intensification is driven by placing a regional forcing with  $z=4$  and  $j_{max}=34\text{m/s}$  along with the mid-latitude forcing. (c) *Control Climate Change Experiments CC(z, j<sub>max</sub>)*, in which a set of experiments are designed where the role of different  $\bar{u}$  and  $z$  in driving the mode 2 related Rossby wave and its persistence over the Indian region is done. (d) *Sensitivity Climate Change Experiments SC(z, j<sub>max</sub>)*, where the role of different  $\bar{u}$  and  $z$  in causing intensification of mode 2 related circulation over the Indian region is done. The summary of the set of experiments is provided in **Table 1**. The model is integrated with a time step of 900 s and the output is saved every 6 hrs. The maximum jet speed for control  $C(4,34)$  is assumed based on the observed climatological maximum jet speed over the subtropical region during the April-May period.

Experiment Name	Vorticity Forcing	Stationary Wave Number ( $z$ )	Maximum Jet Speed ( $j_{max}$ ; Corresponding to zonal mean wind)	No. of Experiments
<i>Control</i> <i>C(4,34)</i>	1 (Mid-latitude)	4	34 m/s	1
<i>Control</i> <i>Climate</i> <i>Change</i> <i>CC(z,j<sub>max</sub>)*</i>	1 (Mid-latitude)	1,2,3,4,5,6,7,8	22,26,30,34,42,50,60,70 m/s	64 (including C(4,34))
<i>Sensitivity</i> <i>S(4,34)</i>	2 (Mid-latitude+ Tropical)	4	34 m/s	1
<i>Sensitivity</i> <i>Climate</i> <i>Change</i> <i>SC(z,j<sub>max</sub>)*</i>	2 (Mid-latitude+ Tropical)	1,2,3,4,5,6,7,8	22,26,30,34,42,50,60,70 m/s	64 (including S(4,34))

\*For each stationary wave number pattern ( $z=1,2,3,4,5,6,7$  and  $8$ ), the model is prescribed maximum jet speeds  $j_{max}=22,26,30,34,42,50,60$  and  $70$  m/s. Total number of experiments=128.

**Table 1:** Set of experiments conducted using the barotropic vorticity equation model framework

The linear regression model is used to estimate the temperature and humidity from the vorticity patterns. The linear regression for temperature and RH at any time step,  $t$  is of the form,

$$T(lat, lon) = m_T(lat, lon) \times \zeta(lat, lon) + C_T(lat, lon)$$

$$RH(lat, lon) = m_{RH}(lat, lon) \times \zeta(lat, lon) + C_{RH}(lat, lon)$$

The regression coefficients ( $m_T$  and  $m_{RH}$ ) and constants ( $C_T$  and  $C_{RH}$ ) were obtained from the observed relative vorticity at the upper level, the surface temperature and RH for a period from 1980-2020. Thus, the obtained slope and constants are used to evaluate the temperature distribution from the barotropic model predicted vorticity. The same procedure is followed for relative humidity, and the HI is then calculated from the estimated temperature and humidity.

This study measures intensification as a function of amplification and persistence. This can be looked at as follows. Mode 2 can amplify sharply due to Rossby wave amplification, which can cause large departures of temperatures above normal for a short period. Similarly, in other cases, mode 2 may not be too much amplified but can persist over a region for a longer time. This can also cause temperature departures above normal for a large number of days. Or it may be a mixture of both of the above scenarios. Considering the possibility of both these factors, intensification in this study is considered a function of both amplification and persistence.

## 4. Results

### 4.1 Observed Mode 2 Intensification over the Indian region

Here, the modal signatures in the dynamic and thermodynamic parameters, which represent the observed intensification over the Indian region, are analyzed. The composite of actual surface temperature and vorticity anomaly at 200hPa for those days when PC 2 > 1.0 ('*active mode 2*' days) is shown for days lagging from -7 to a lead of 1 with respect to active mode 2 days. There is an anticyclonic-cyclonic circulation pattern (**Fig 3a**), which intensifies from lag -5 onwards over the northern parts of the Indian region. **Fig 3b** shows the spatial composite of actual temperature, which depicts the rise in temperature over the North-West Indian (NWI) region, especially from lag -4 days onwards, clearly responding to the intensified circulation pattern. Now for a clearer picture of the intensification of the upper-level anticyclonic anomaly and the maximum temperature, the composite of average vorticity over the NWI region (27-30 °N; 72-75 °E) at 200hPa and standardized maximum temperature anomaly are plotted from lag -7 to lead 2 with respect to the active (PC 2 > 1.0) and extreme (PC 2 > 2.0) mode 2 days (**Fig 4**). In both cases, an apparent intensification of upper-level vorticity on the negative side (depicting anticyclonic circulation) and associated rise in standardized maximum temperature anomaly is evident over the NWI region (**Fig 4a** and **4b**). **Fig 4c** and **4d** show the percentage of grid points that showed maximum temperature value greater than 40 °C ( $T_{max} > 40$  °C) for days from lag -7 to lead 2 for the same region as in **Fig 4a** and **4b**. It shows a gradual rise in the spatial extent of the region with  $T_{max} > 40$  °C from lag -7 onwards (**Fig 4c**), with a steeper rise for extreme days (**Fig 4d**). By considering both the amplification and persistence of the system, it is seen that mode 2 circulation shows a distinct intensification pattern resulting in a rise in temperature over the Indian region. The anticyclonic vorticity structure (**Fig 3a**) observed over the Northwest Indian region during active mode 2 days clearly shows barotropic structure as seen in **Fig 4e**. It is also to be noted

from **Fig 3a** that there is a strong cyclonic circulation associated with mode 2 along the Eastern Coastal regions in India. In the pre-monsoon summer season, the Bay of Bengal (BoB) is expected to be warm enough to support local-scale convective systems. This is evident from the sea-surface temperature (SST) and vertically integrated moisture flux (IMF) anomalies (**Fig 5**) for active and extreme mode 2 days. The SST anomaly shows a distinct warming over the southernmost BoB, especially close to Indonesia. Apart from that, there is a strong moisture influx towards the eastern coastal to central Indian region, further weakening towards the interior landmass. This hints towards two possible conditions associated with mode 2 and its intensification: (a) Warm SST (especially in the southernmost BoB) can act as a regional heat source, and (b) strong regional scale circulation pattern (as seen from IMF) can bring moisture supply to Indian landmass which could lead to humid heat stress (given the high-temperature conditions). To understand the mode 2 teleconnection pathway and its intensification over the Indian region, the role of the SST pattern and the regional circulations are also to be considered. Such a kind of understanding can be developed based on model studies. Here, we are thus approaching this mode 2 Rossby wave-related heatwave intensification using a simple yet powerful model, the non-divergent barotropic vorticity equation.

#### **4.1 Mode 2 Teleconnection Pathway and its Intensification in a Barotropic Model**

In this section, we will be using a dynamical model that uses the non-divergent barotropic vorticity equation, with prescribed initial conditions (discussed in detail in Section 2) to drive (a) Mode 2 teleconnection pathway and (b) Mode 2 intensification. These experiments aim to understand the appearance of mode 2-related anticyclonic circulation, its amplification and persistence, and thereby, intensification over the Indian region, which helps us understand the heatwave intensification over India.

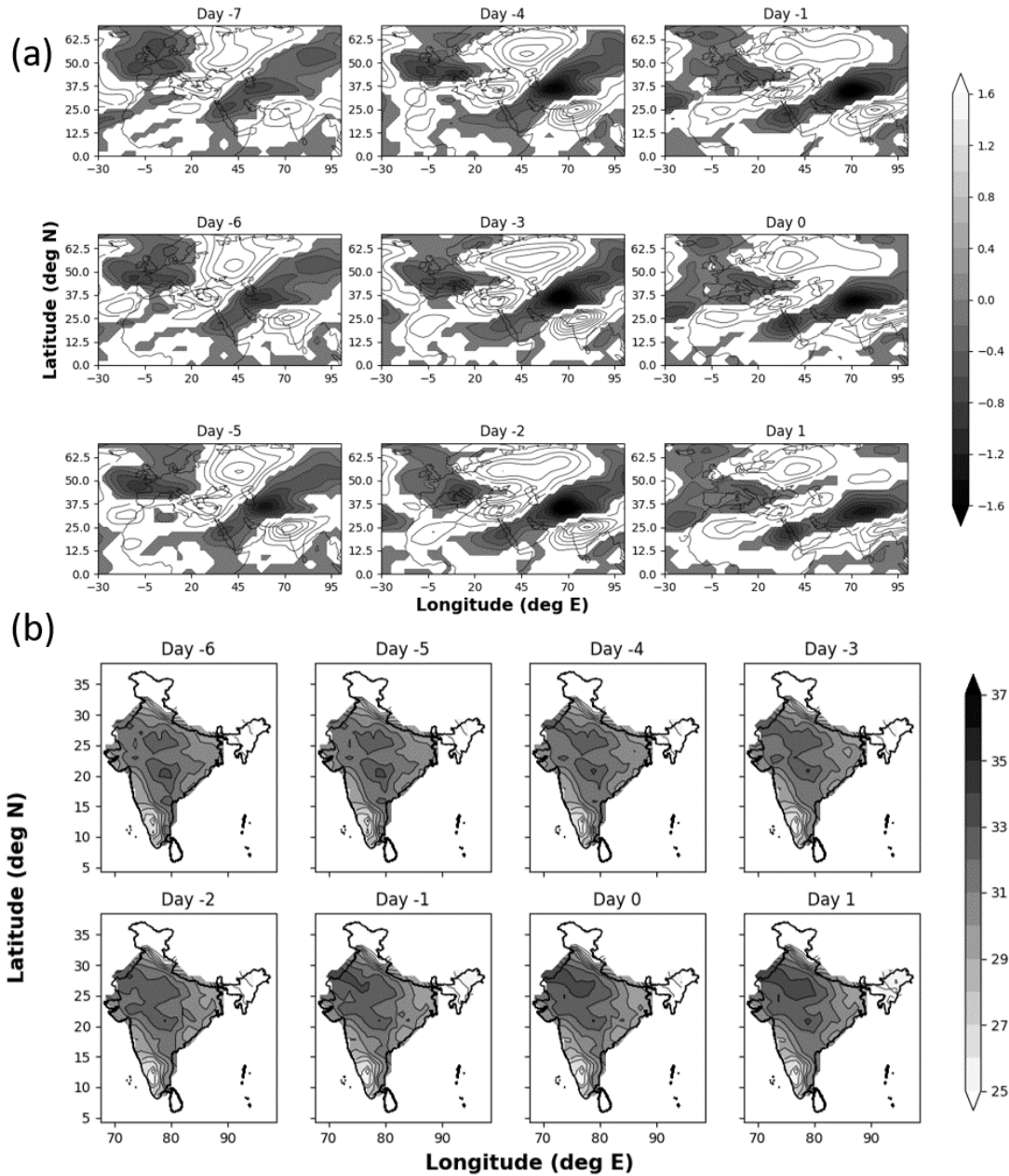


**Figure 3:** (a) Spatial composite of relative vorticity anomaly at 200 hPa for active mode 2 days ( $PC_2 > 1.0$ ) from lag -7 to lead 1 day with respect to active mode 2 days. (b) Spatial composite of actual surface temperature for active mode 2 days in the same way as shown in Fig3a.

#### 4.1.1 Mode 2 Propagation and Persistence over the Indian Region

In a previous study, it was found that Rossby waves propagate through the *Europe-Middle East-Indian Ocean* pathway when the forcing was put in the tropical eastern Pacific close to the west coast of North America (Fig 2b of (Ambrizzi and Hoskins 1997)). Later in LC22, the mode 2 Rossby waves were found to follow a remarkably similar pathway and

reach over the Indian region, with a clear signature starting from the western Coast of Europe (Fig 9 of LC22). The vertical profile of the vorticity pattern over this region (50-70 °N; 5-25 °W) shows a dominant barotropic structure, making it suitable for applying as a forcing in the barotropic model. So, in the  $C(4,34)$  experiment (Refer **Section 2**), an anticyclonic stirring in the form of a stationary circular vorticity forcing below Iceland close to the west coast of Europe was provided as in **Fig 2d**. The model response from  $t=72$  hrs. up to  $t=192$  hrs. is shown in **Fig 6**. It is seen that a cyclonic-anticyclonic vorticity structure is propagating from the source region, which is further elongating and propagating over the northern Indian region, peaking during  $t=92$  to 120 hrs. and later weakening but persisting over North India. This structure closely resembles the observed vorticity pattern, as shown in **Fig 3a**. Thus, the anti-cyclonic vorticity forcing, which is consistent with the observed barotropic anticyclonic vorticity anomaly (**Fig 2a**), can drive the mode 2 teleconnection pathway that produces the circulation anomalies that propagate and reaches the North-Indian region.

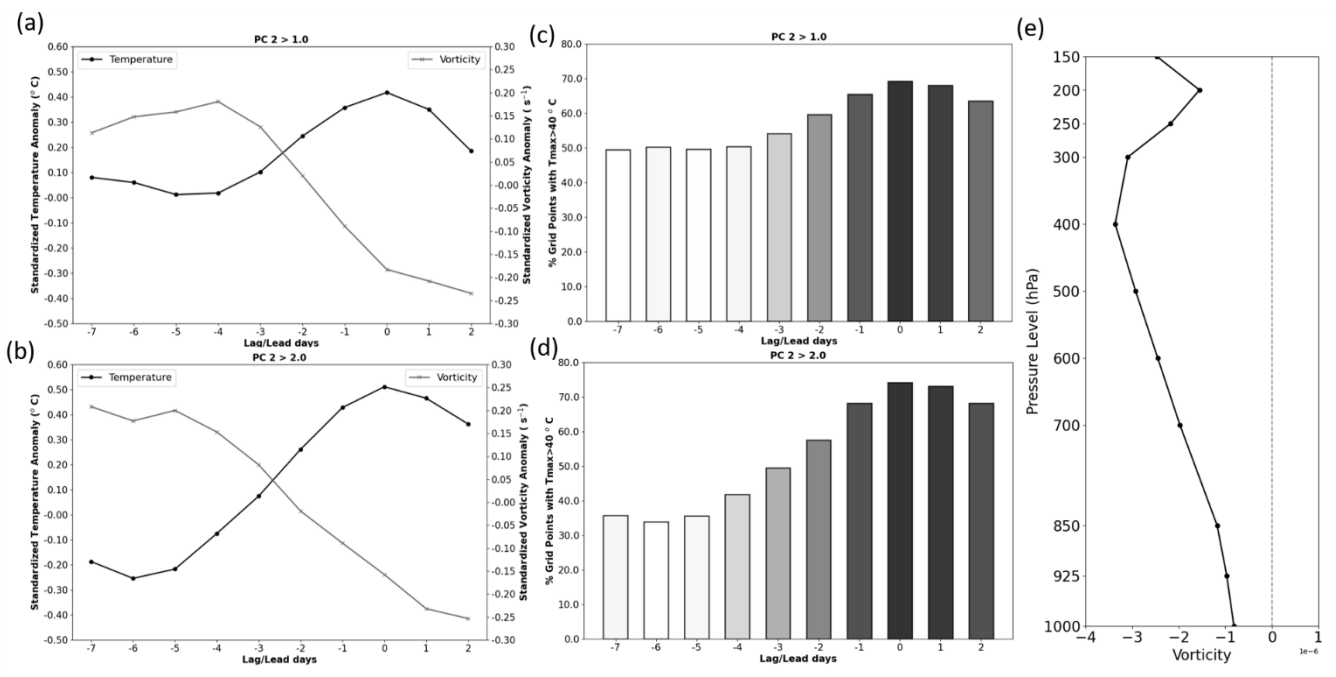


**Figure 4:** Composite of the standardized anomaly of relative vorticity at 200 hPa and maximum temperature for **(a)** Active mode 2 days ( $PC\ 2 > 1.0$ ) and **(b)** Extreme Mode 2 days ( $PC\ 2 > 2.0$ ) over the Northwest Indian region (27-30 °N; 72-75 °E) during different lags during April-May from 1980-2020. Percentage number of grid points at different lags with maximum temperature > 40 °C for **(c)** Active Mode 2 days and **(d)** Extreme Mode 2 days **(e)** Vertical profile of area-averaged observed relative vorticity over the North-Central Indian region (23-33 °N; 75-85 °E) for active mode 2 days.

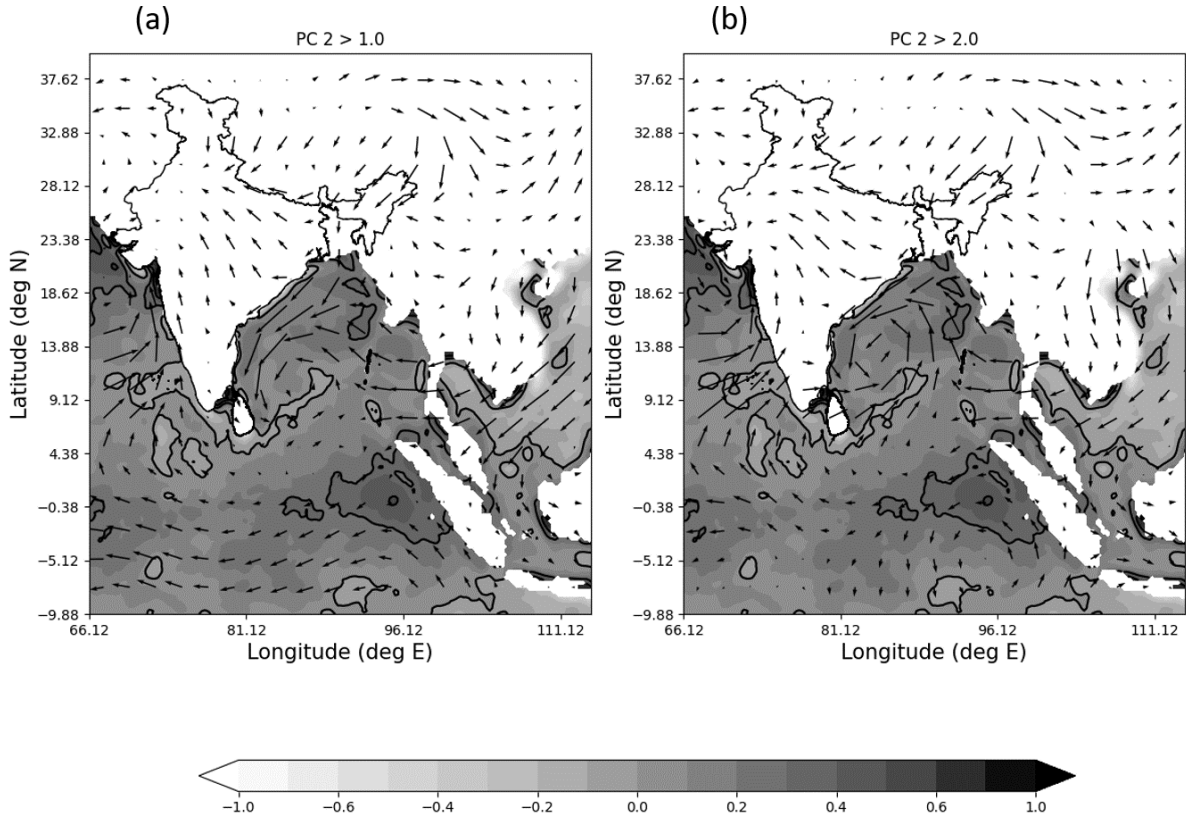


**Figure 5:** Composite of sea surface temperature superimposed with vertically integrated moisture flux (IMF) from 1000-300 hPa for **(a)** Active Mode 2 days and **(b)** Extreme Mode 2 days during April-May from 1980-2020.

#### 4.1.2 Mode 2 Response to a Local Forcing over BoB

The anticyclonic vorticity forcing on the western coast of Europe can induce the mode 2-related teleconnection pattern, which is consistent with the observed upper-level circulation features. This mode, which partly drives the intraseasonal variability of summer temperature over the Indian region, occasionally intensifies, which could lead to heatwaves. Given the increasing long-term trend (**Fig 1b**) of mode 2, it is important to understand what causes the intensification of this mid-latitude Rossby wave over the Indian region. From the observation, it is hypothesized that a local heat source over the southernmost BoB (**Fig 5**) can provide favorable conditions for mode 2 intensification. Also, the composite of vorticity anomaly over a tropical region (0-20 °N; 80-95 °E) for different levels (dotted line in **Fig 2a**) evidently shows a cyclonic structure, which is barotropic in nature. Thus, a local cyclonic vorticity forcing is provided over the southernmost part of BoB, along with the mid-latitude Rossby wave forcing ( $S(4,34)$ ). The model vorticity response to the applied IC conditions from a lead time  $t=72$  hrs. to  $t=192$  hrs. is shown in **Fig 7**. The time steps  $t=120$  hrs, 144 hrs, and 168 hrs. show clear signatures of the superimposing of the anticyclonic

phase of the eastward propagating mid-latitude Rossby wave and the north-westward propagating anticyclonic pattern over the Indian region. The anticyclonic phases superimpose over each other in the northwest-central Indian region, giving rise to an intensified anticyclone, which later propagates southwestward. Earlier studies have identified similar mechanisms as a major cause of Rossby wave amplification (Shaman and Tziperman 2016).

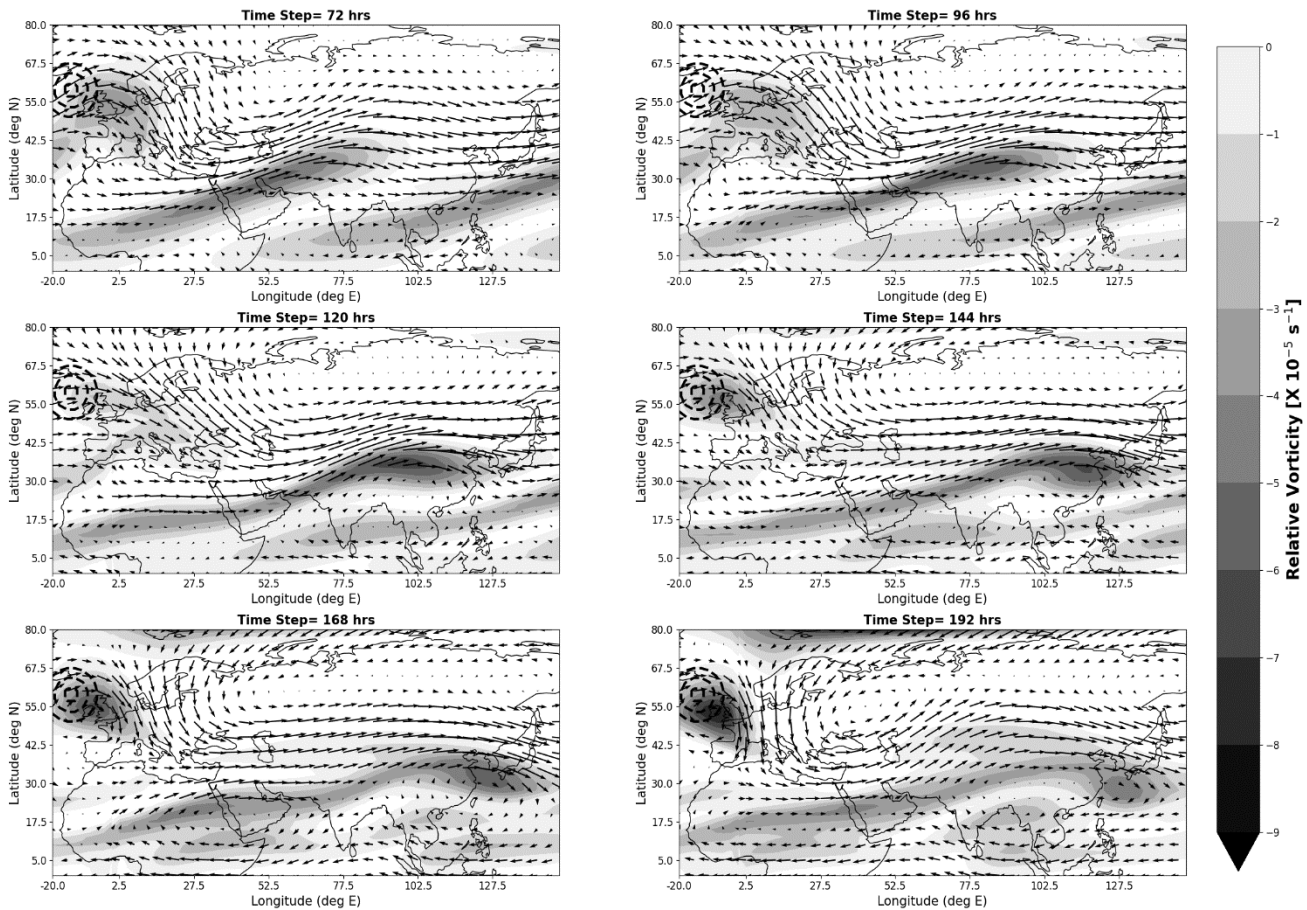


**Figure 6:** Barotropic Model predicted vorticity at different time steps from  $t=72$  hrs to  $t=192$  hrs for the  $C(4,34)$  control experiment.

To look further at the superimposing of waves, the Hovmöller diagram of vorticity is plotted and compared with the observational vorticity anomaly pattern. **Fig 8a** shows two Hovmöller diagrams of observed vorticity anomaly composite, one overlaid over the other in which the shaded part gives the propagation of mid-latitude Rossby wave (averaged over latitude belt of 35-40 °N). Above that, another Hovmöller diagram (averaged over latitude belt 5-15 °N) showed in red contour lines is plotted, which shows the westward propagating anticyclonic pattern from the tropics. The composite is made from a lag of -7 days to a lead time of 2 days with respect to extreme mode 2 days (PC 2 > 2.0). It can be seen that the anticyclonic vorticity superimposes over the Indian region, peaking around lag=2 to lead=1 with respect to extreme mode 2 days. The model experiment also shows clear evidence of the

superimposing of both the anticyclones over the Indian region, similar to the observed pattern (**Fig 8b**). Thus, a cyclonic forcing over the southernmost BoB can lead to the superimposing of these oppositely directed patterns in the Indian region. So, does superimposing lead to the intensification of mode 2? This is explained in **Fig 8c** and **8d**. The density distribution of vorticity over the Indian region (15-40 °N and 70-90 °E) during the model time steps from  $t=72$  to  $t=216$  hrs. is provided for  $C(4,34)$  and  $S(4,34)$ . The distribution of  $S(4,34)$  shows a shift in the vorticity towards more negative values than the same for  $C(4,34)$ . This shows that amplification of model anticyclonic vorticity over the Indian region occurs by placing a cyclonic forcing over the southernmost BoB. Also, it is seen that amplified anticyclonic vorticity (below a reference threshold of  $-2.0 \times 10^{-5} \text{ s}^{-1}$  as obtained from observed vorticity) is observed for a higher percentage of model time steps in  $S(4,34)$  than in  $C(4,34)$ , indicating its persistence over the Indian region (**Fig 8d**). Thus, one of the dynamic mechanisms by which mode 2 related Rossby wave amplifies is the superimposition of anticyclonic phases of the mid-latitude Rossby wave and westward propagating equatorial anticyclonic pattern generated by the cyclonic forcing. So, the regional forcing over BoB plays a dominant role in the intensification of the mid-latitude mode 2 teleconnection pathway by causing amplified and persisting anticyclonic patterns over the Indian region. The westward propagation of the pattern also hints towards the moisture influx to the east coast, as observed for mode 2 (**Fig 5**). That is, this dynamical mechanism of mode 2 Rossby wave intensification also explains the behavior of mode 2 being a cause of humid heat stress over the Indian region.

#### **4.2 Sensitivity of Mode 2 Teleconnection and its Intensification on the Stationary wave pattern and zonal jet**

From the climate change perspective, the dynamical mechanism of the mode 2 teleconnection pathway and its intensification over the Indian region has to be understood. Studies have shown that the summertime stationary waves in the Northern Hemisphere tropics are projected to weaken (Wills et al. 2019). But in the subtropics, for a high emission scenario, especially over northwestern North America, the stationary circulations are projected to strengthen (Zhang et al. 2023). Thus, it is necessary to understand the impact that will be caused by the background conditions, such as the stationary waves and the zonal wind pattern on intensification. Also, the weakening of the jet stream due to weakened meridional thermal gradient and their link with extremes are also a topic of discussion recently. Here, these two aspects are studied based on the current modeling framework. **Fig 9** gives the density distribution of vorticity over the Indian region (Box: 15-40 °N; 70-90 °E) for the

model time steps from  $t=72$  to  $t=216$  hrs. In the figure, the density distribution of vorticity for  $CC$  and  $SC$  for each  $\bar{u}$  and  $z$  configuration is provided for comparison. The  $j_{max}$  corresponding to each  $\bar{u}$  is provided in the figure. It can be seen that the distribution of vorticity for  $SC$  is shifted towards more negative values as compared to  $CC$  for almost all  $z$  patterns (3,4,5,6) while the  $j_{max}$  is lower. As  $j_{max}$  increases, there is no distinguished difference between the distribution of vorticity for the  $CC$  and  $SC$  experiments and vorticity is shifting towards positive ranges pointing towards the weakening anticyclonic circulation. That is, for lower  $j_{max}$  conditions, the anticyclonic vorticity over the Indian region is amplifying in the presence of a tropical forcing and for the higher ranges, amplification is not evident and the anticyclonic phase is also weakening for almost all  $z$  patterns (3,4,5,6).

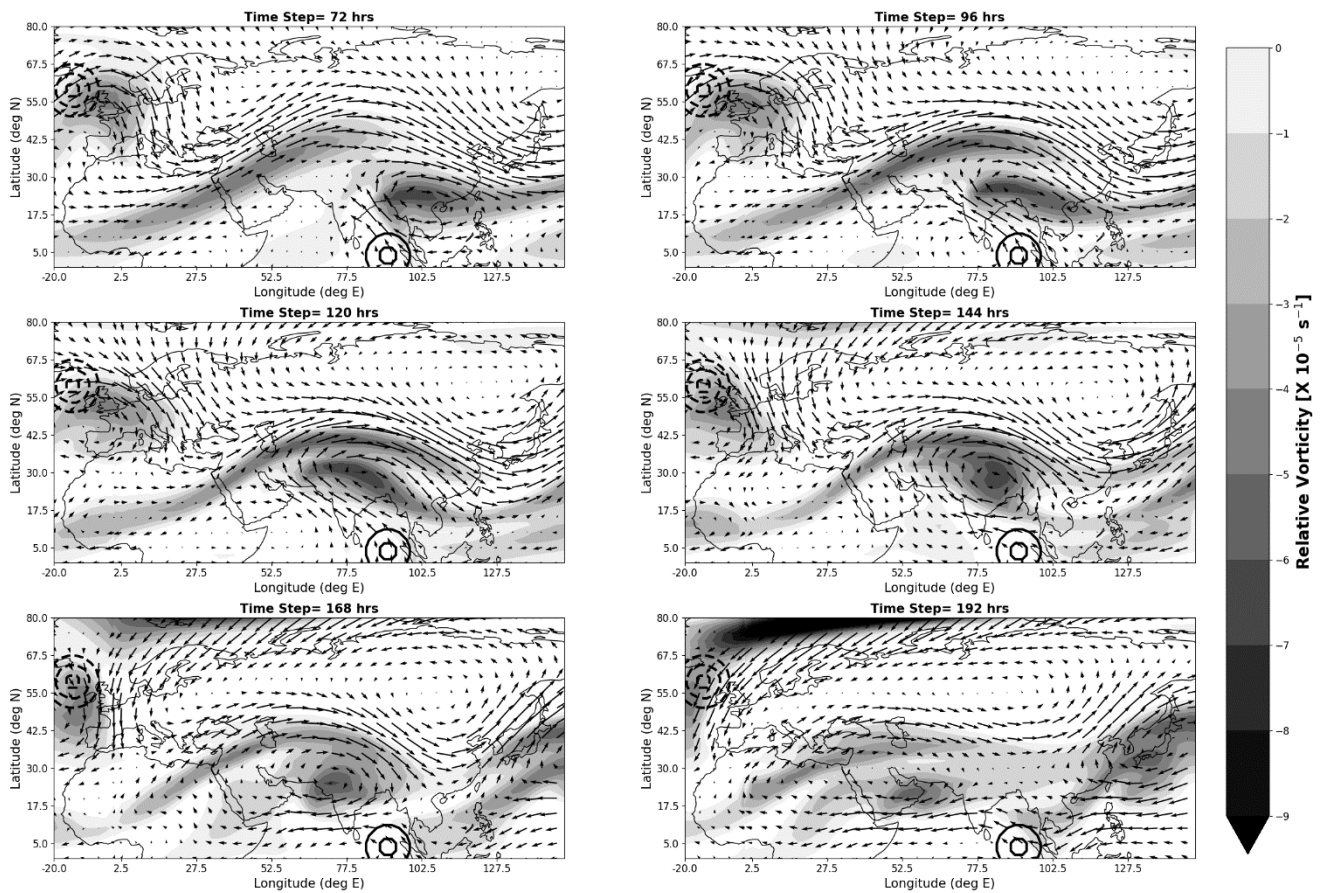


**Figure 7:** Barotropic Model predicted vorticity at different timesteps from  $t=72$  hrs. to  $t=192$  hrs. for the  $S(4,34)$  sensitivity experiment.

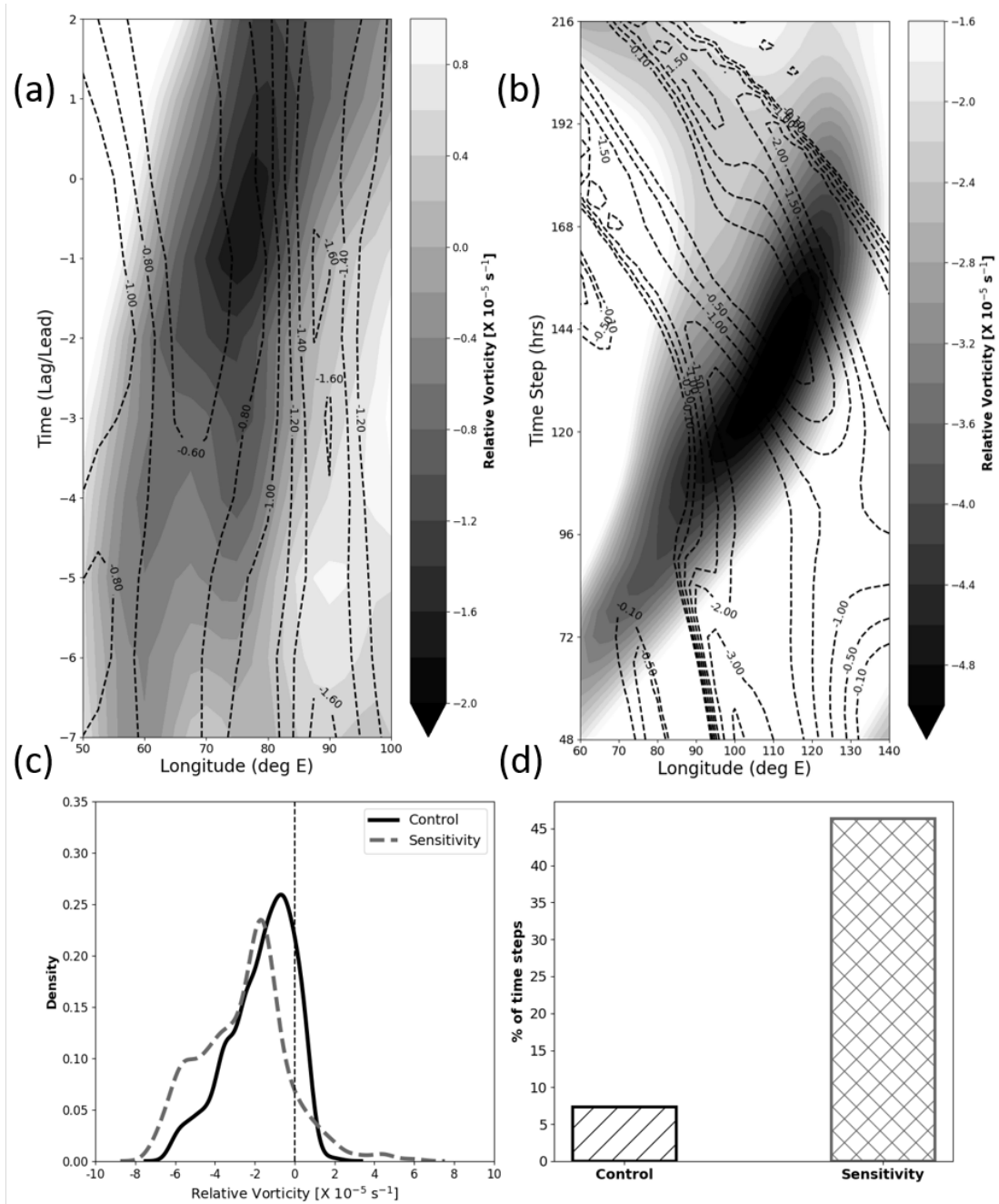


**Figure 8:** (a) Hovmöller diagram of observed relative vorticity anomaly composite at 200 hPa averaged over latitude belt of 35-40 °N (shaded) overlaid by Hovmöller diagram of the same averaged over the latitude belt of 5-15 °N (contour lines) for days lagging from -7 to lead 2 with respect to active mode 2 days. (b) Hovmöller diagram of the model predicted vorticity from t=48 hrs. to t=216 hrs. averaged over the same latitude belts as in **Fig 8a**. (c) Density distribution of vorticity over the Indian region (15-40 °N and 70-90 °E) for model time steps from t=72 to t=216 hrs. for  $C(4,34)$  and  $S(4,34)$ . (d) Percentage of time steps when the average of vorticity over the Indian region falls below  $-2.0 \times 10^{-5} \text{ s}^{-1}$  for  $C(4,34)$  and  $S(4,34)$ .

To look at the persistence of the circulation over the Indian region, the frequency of model timesteps (%) when the average vorticity over the Indian region was below  $-2.0 \times 10^{-5} \text{ s}^{-1}$  is plotted (**Fig 10**). The frequency is calculated for all the *CC* and *SC* experiments. It is clear from **Fig 10** that the Rossby wave propagates through the mode 2 teleconnection pathway, and the associated anticyclonic vorticity persisted over the Indian region for the experiments with  $j_{max}=26,30$  and  $34$  m/s for almost all  $z$  patterns. This is also true for the amplified wave due to superimposing Rossby waves, with the persistence of anticyclonic vorticity over the Indian region extending to more than 30-40% of model time steps. As  $j_{max}$  increases, the average vorticity below the threshold for both *CC* and *SC* experiment diminishes and becomes nil when  $j_{max}$  rises to  $70$  m/s. In general, the persistence of anticyclonic vorticity over the Indian region for the *CC* experiment is maximum when  $j_{max}=26,30,34$  m/s. In these  $\bar{u}$  configurations, the persistence shows variations among different values of  $z$ . At the same time, the same for the *SC* experiments are maximum when  $j_{max}=22,26,30$  and  $34$  m/s with  $z$  in the range of 2-6. Thus, by considering the amplification of anticyclonic circulation associated with mode 2 Rossby wave (**Fig 9**) and also its persistence over the Indian region, we can summarize that the intensification is favored more for the configurations where  $j_{max}= 26-34$  m/s and  $z=2,3,4,5$  and  $6$ . Above and below these limits the mode 2 associated Rossby wave intensification is not favored in the current modeling framework.

A summary of the favorable conditions that can lead to intensified anticyclonic vorticity over the Indian region caused by superimposition is provided in **Fig 11**. The figure shows the ratio of the average vorticity over the Indian region between the *SC* and the *CC* experiments. Here, while calculating the ratio, the anticyclonic vorticity intensification in the *SC* experiment is only considered. The magnitude gives how many times the anticyclonic vorticity got intensified over the Indian region in the presence of the regional forcing in BoB. The combinations of  $z$  and  $\bar{u}$  (or  $j_{max}$ ) favorable for such a superimposition and intensification of mode 2 Rossby wave are evident from **Fig 11**. Once such an anticyclonic circulation reaches the Indian region, this can cause a sinking air motion, leading to a clear sky and adiabatic warming of air. An intensified circulation that persists over the region for a longer time can drive the temperature extremes over the Indian region, causing intensified heatwaves.

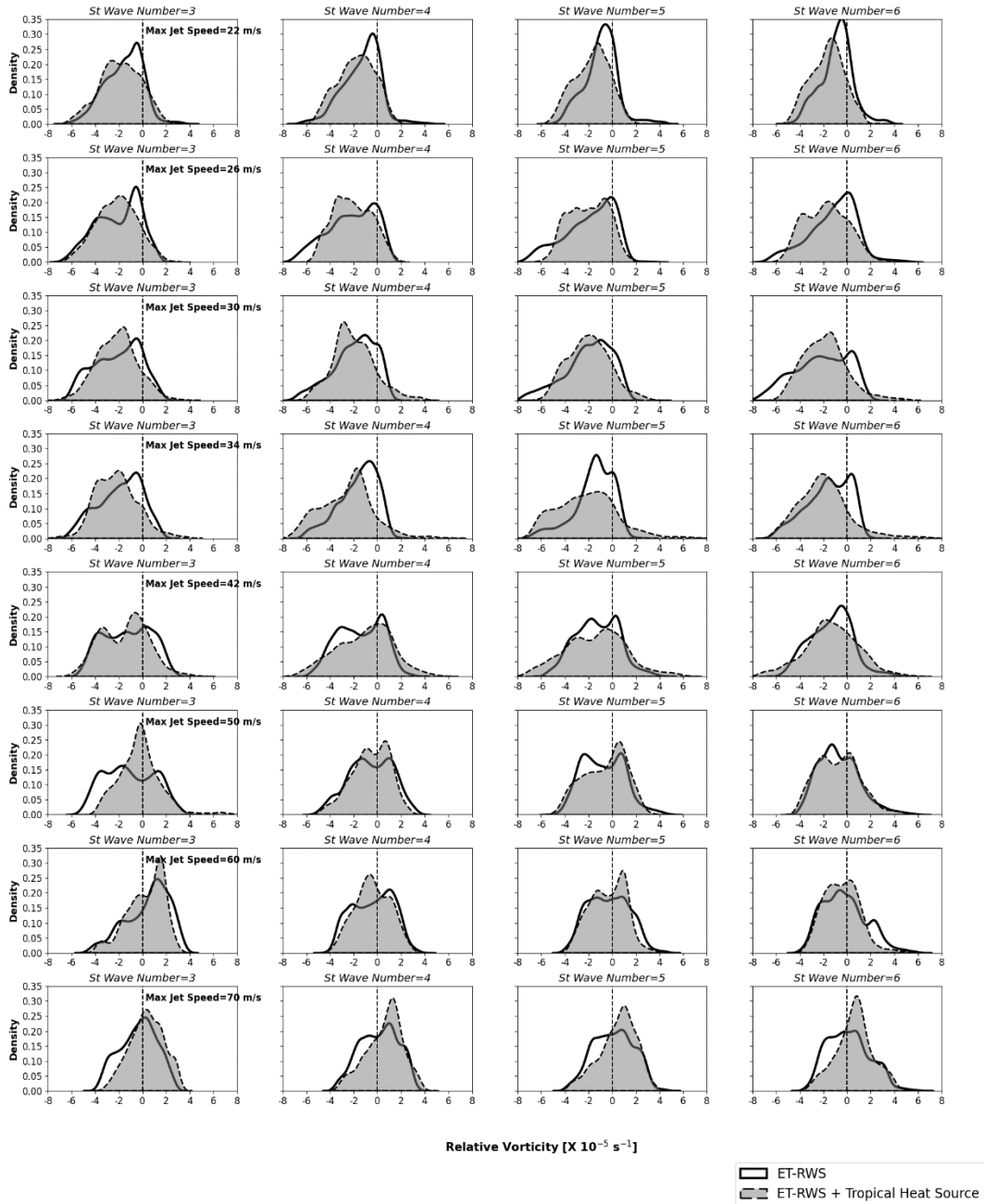


**Figure 9:** Density distribution of relative vorticity over a box in the Indian region (15-40 °N; 70-90 °E) for model time steps from t=72 to t=216 hrs. for different CC (ET-RWS) and SC(ET-RWS + Tropical Heat Source) experiments. Each row represents a particular set of zonal wind configurations, with each column representing different wave numbers.

### 5. Mode 2 Intensification and Temperature Extremes over Indian region

In the previous sections, using the barotropic model, the vorticity response of the model to the vorticity perturbations in the midlatitudes and the Bay of Bengal was examined. A linear regression model is used to understand the evolution of temperature in response to the vorticity. The temperature at different lead time steps, as estimated from the barotropic model

predicted vorticity, is given in **Fig 12**. A similar estimation is done for the RH pattern over the Indian region. From the estimated temperature and RH, the HI is calculated for analysis. An intensification of the temperature over the North-west and Central Indian region associated with intensified anticyclonic vorticity (in the presence of forcing over BoB) is noted in **Fig 12b** as compared to **Fig 12a** (without forcing over BoB), especially in the lead time of  $t=96$  hrs. to  $t=168$  hrs. Thus, the intensification of the mode 2 teleconnection pattern (as seen from vorticity) causes an intensified response in temperature, which can lead to extreme temperature conditions such as heatwaves. In addition to the temperature, it is also seen that the heat stress over the Central Indian region also shows intensification in the  $S(4,34)$  experiment. The probability distribution of the difference in temperature and HI ( $S(4,34) - C(4,34)$ ) over the Northwest and Central Indian regions (**Fig 12c**) shows a clear sign of intensification associated with the intensified anticyclonic circulation.

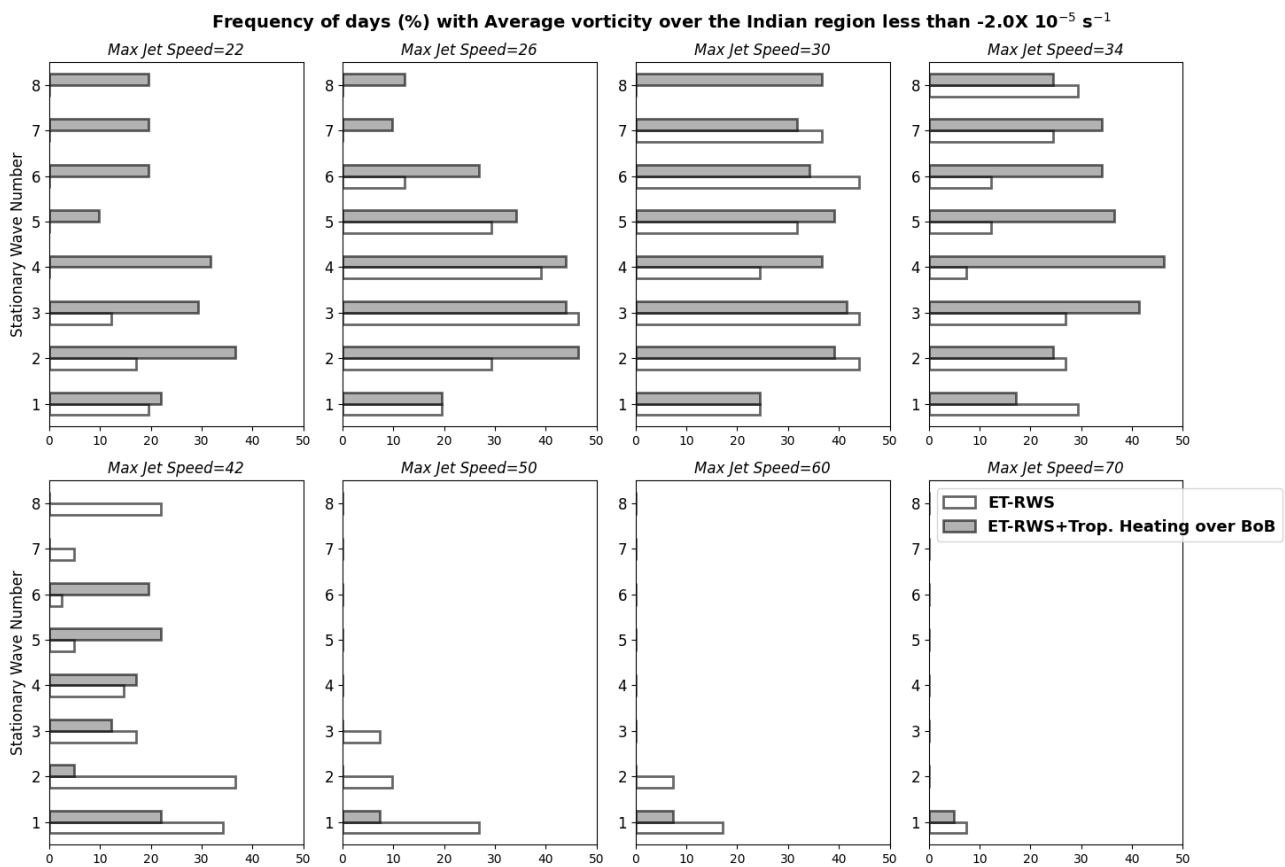


**Figure 10:** Percentage frequency of model time steps when the average vorticity over the Indian region falls below  $-2.0 \times 10^{-5} \text{ s}^{-1}$  for each CC (ET-RWS) and SC (ET-RWS + Tropical Heat Source) experiments. Each subplot represents a different zonal wind configuration.

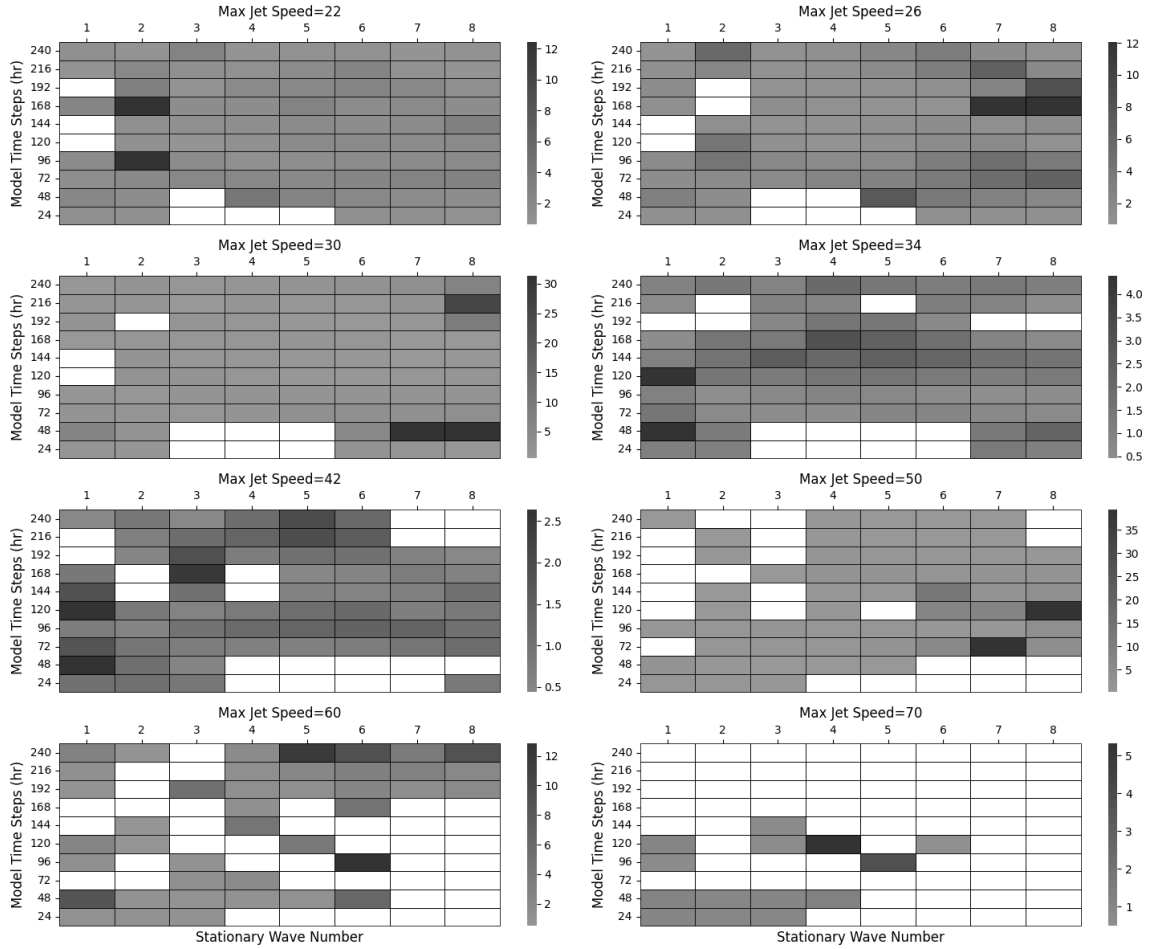


**Figure 11:** Heatmap of the ratio of the average anticyclonic vorticity over the Indian region between the SC and the CC experiments at different time steps (y-axis) and different zonal wavenumbers (x-axis). White boxes represent the non-existence of anticyclonic vorticity in the respective SC experiment for different time steps. Each panel represents a different zonal wind configuration with the maximum zonal jet speed mentioned at the top.

## 6. Summary and Discussions

The major objective of the current study is to understand what causes the intensification of temperature sub-seasonal variability resulting in intensified heatwaves over the Indian region. Temperature variability over India has two dominant modes during the summer season driven by mid-latitude Rossby waves (LC22). An amplification of these Rossby wave modes occurs over the Indian region, driving a significant number of extreme temperature events. However, it was not clear if the amplified heatwave modes arise due to teleconnection modes alone or if some regional forcing contributes to the amplification. As shown earlier (Lekshmi et al., 2024), while the first mode does not correlate well with the

moisture distribution pattern over the Indian region, the second mode, with a strong regional response, is associated with a huge supply of moisture, especially in the East Coast, from the Bay of Bengal. It was shown that such local moisture patterns can lead to severe humid heat stress conditions, which, when amplified, could prove fatal for health. Also, the moist (second) mode is showing a significantly increasing trend over the Indian region, thus making the interpretation imperative. These evidences lead to the hypothesis that local forcing may contribute to the amplification of heatwaves over India through locally mediated amplification of extratropical Rossby wave modes intruding over the Indian region. With the use of the non-divergent barotropic vorticity model, forced by a local and extratropical forcing, this work thus focuses on the dynamical process behind the amplification of the second mode and associated circulation, which can lead to the intensification of the heatwaves over the Indian region.

In this study, it is found that the intensification is the result of regionally forced wave amplification and persistence over any particular region. Experiments are conducted to understand the dynamical mechanism associated with the mode-2 teleconnection pathway, their propagation, and the persistence of the anticyclonic phase over the Indian region. It was found that forcing the non-divergent barotropic vorticity equation using anticyclonic circulation close to the western coast of Europe (as seen from the observation pattern) drives the mode-2 related Rossby waves and their propagation (**Fig 6**). Furthermore, there is a strong regional response for mode 2 (**Fig 1 and 3a**), which is evident from the SST pattern and the moisture influx towards the eastern coastal states (**Fig 5**). Based on this evidence from the observation, a cyclonic vorticity forcing is provided in the southernmost BoB, close to the coast of Indonesia, along with the mid-latitude Rossby wave source. It was found that intensification of the anti-cyclonic vorticity over the Indian region is occurring by the superimposition of the westward propagating anticyclonic pattern and the eastward propagating mid-latitude Rossby wave (**Fig 7 and 8**). The anticyclonic phase of both waves is superimposing and persisting over the northern-central Indian region and later moving southwestwards. Such a superimposition mechanism is known to cause the amplification of Rossby waves (Shaman and Tziperman 2016). As a result of the barotropic nature, the intensified anticyclonic circulation causes subsidence motion of air and further formation of clear skies, leading to adiabatic warming of air. Also, the intensified mode 2 pattern demonstrates that circulation can favor the moisture influx towards the coastal states (**Fig 7**), similar to that from the observation (**Fig 5**), which drives the humid heat stress over that

region. With the aid of a linear regression model, the temperature and the RH are estimated from the barotropic model predicted vorticity. The distribution of HI obtained from the estimated temperature and RH shows a clear indication of intensification occurring over the Indian region associated with the intensified anticyclonic vorticity. Apart from the large-scale vorticity pattern, the impact caused by the regional circulation favors the inflow of humidity towards the Indian landmass, thus driving the intensification of heat stress. This is the novelty of the study in which the dynamical mechanism of the intensification of the circulation features (which is predominantly barotropic in nature) is simplified by using the barotropic model but still able to evaluate the temperature patterns and regional heat stress without actually involving the complexities of a baroclinic model.

Climate change plays both a direct and indirect role in driving the temperature extremes over any region. While the direct role can be attributed to the rise in mean temperature, the indirect role is through the changes in the background stationary wave patterns, mean zonal wind pattern, location and speed of jetstream, etc. The interaction of these features and the resultant extreme event are highly non-linear in nature and require further understanding (Palmer 2013; White et al. 2022). In the aspect of wave amplification, this understanding usually provides us with a set of ‘*weather regimes*’ (defined here as patterns associated with stationary wave and zonal mean wind combinations) where the Rossby wave amplification is more favored. Here, we found that the superimposing waves can lead to more intensified Rossby waves, especially when  $z=3,4,5$  and  $6$  and  $j_{max}=26,30$  and  $34$  m/s (Fig 9 and 10). Such preferential selections are likely to occur as a result of highly non-linear processes. A summary of the *weather regimes* that prove to be favorable for the intensification of mode 2 Rossby waves is shown (Fig 11). However, care must be taken while linking the intensified (amplified & persisting) Rossby waves with extreme events. Because intensified waves can cause anomalously warm conditions in particular locations, and at the same time, they can cause anomalous cooling at other locations as well. That is, global warming can favor local cooling (Palmer 2013). From Fig 11, along with the regimes where the anticyclonic circulation intensifies (in the presence of tropical forcing), a glimpse of other regimes where the cyclonic circulation could intensify is also seen (which is given as the white boxes). Such type of conditions can lead to intense cyclonic circulation and the formation of local-scale thunderstorms because of the moisture availability as part of mode 2 over the eastern coastal states. These types of scenarios are not uncommon during the pre-monsoon season in the coastal states of India but are out of the scope of the present study. The current study, though

based on a very simple Rossby wave superposition paradigm, provides a simple dynamical mechanism in which the Rossby wave associated with mode-2 teleconnection intensifies, leading to the intensification of heatwaves in the Indian region.

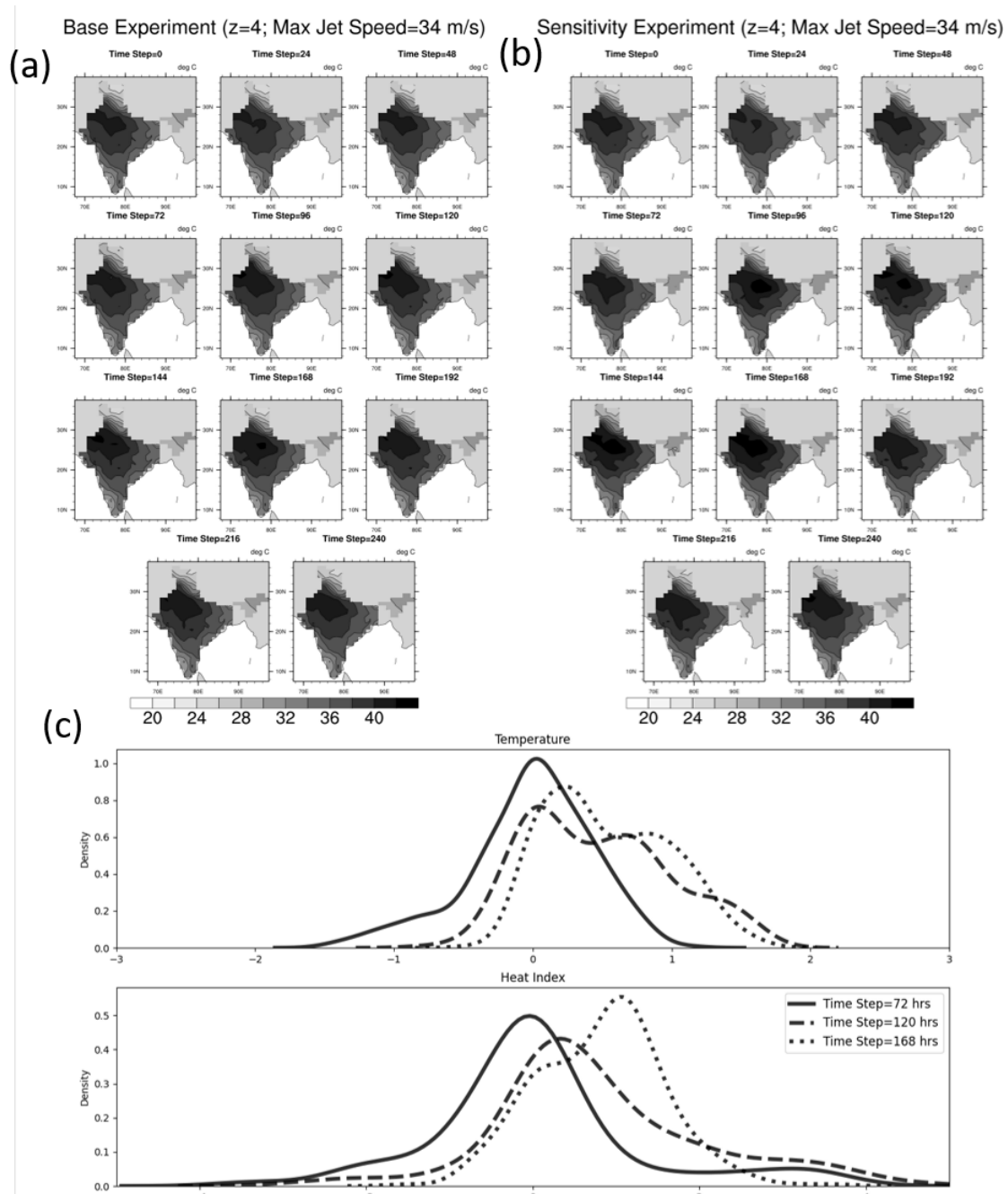


**Figure 12:**(a) Linear Regression Model estimated temperature pattern from the barotropic model relative vorticity at different time steps for  $C(4,34)$  experiment. (b) Same as Fig 12a for  $S(4,34)$  experiment. (c) Density distribution of the difference in estimated temperature and Heat Index ( $S(4,34) - C(4,34)$ ) for three barotropic model time steps  $t = 72, 120,$  and  $168$  hrs.

## Acknowledgments

The core barotropic model used in the study is based on the Held-Suarez Barotropic model adapted from <https://github.com/lmadaus/Barotropic-Python> and further developed for the current study. We thank the Python code developers for the barotropic model. LS acknowledges the Ministry of Earth Sciences (MoES), Govt. of India, for the research fellowship support from the MRFP Project. Research support from India Meteorological Department (IMD) and Indian Institute of Tropical Meteorology (IITM), an autonomous institute under MoES is also acknowledged.

## Conflict of interest

The authors declare no competing interests.

## Data Availability

All the input datasets used for the analysis are freely available, as mentioned in Section 2. Any computed data/ codes used to generate the plots will be made available on request.

## References

- Alexander, L., 2011: Extreme heat rooted in dry soils. *Nat. Geosci.*, **4**, 12–13, <https://doi.org/10.1038/ngeo1045>.
- Ambrizzi, T., and B. J. Hoskins, 1997: Stationary rossby-wave propagation in a baroclinic atmosphere. *Q. J. R. Meteorol. Soc.*, **123**, 919–928, <https://doi.org/https://doi.org/10.1002/qj.49712354007>.
- Boer, G. J., and S. J. Lambert, 2001: Second-order space-time climate difference statistics. *Clim. Dyn.*, **17**, 213–218, <https://doi.org/10.1007/PL00013735>.
- Coumou, D., V. Petoukhov, S. Rahmstorf, S. Petri, and H. J. Schellnhuber, 2014: Quasi-resonant circulation regimes and hemispheric synchronization of extreme weather in boreal summer. *Proc. Natl. Acad. Sci.*, **111**, 12331–12336, <https://doi.org/10.1073/pnas.1412797111>.
- Dubey, A. K., and P. Kumar, 2023: Future projections of heatwave characteristics and dynamics over India using a high-resolution regional earth system model. *Clim. Dyn.*, **60**, 127–145, <https://doi.org/10.1007/s00382-022-06309-x>.
- Francis, J. A., and S. J. Vavrus, 2012: Evidence linking Arctic amplification to extreme

- weather in mid-latitudes. *Geophys. Res. Lett.*, **39**,  
<https://doi.org/https://doi.org/10.1029/2012GL051000>.
- Ganeshi, N. G., M. Mujumdar, R. Krishnan, and M. Goswami, 2020: Understanding the linkage between soil moisture variability and temperature extremes over the Indian region. *J. Hydrol.*, **589**, 125183, <https://doi.org/10.1016/j.jhydrol.2020.125183>.
- Ganeshi, N. G., M. Mujumdar, Y. Takaya, M. M. Goswami, B. B. Singh, R. Krishnan, and T. Terao, 2023: Soil moisture revamps the temperature extremes in a warming climate over India. *npj Clim. Atmos. Sci.*, **6**, <https://doi.org/10.1038/s41612-023-00334-1>.
- Goyal, M. K., S. Singh, and V. Jain, 2023: Heat waves characteristics intensification across Indian smart cities. *Sci. Rep.*, **13**, 14786, <https://doi.org/10.1038/s41598-023-41968-8>.
- Grimm, A. M., and P. L. S. Dias, 1995: Use of Barotropic Models in the Study of the Extratropical Response to Tropical Heat Sources. *J. Meteorol. Soc. Japan. Ser. II*, **73**, 765–780, [https://doi.org/10.2151/jmsj1965.73.4\\_765](https://doi.org/10.2151/jmsj1965.73.4_765).
- Guleria, S., and A. Gupta, 2016: *Heat Wave in India Documentation of State of Telangana and Odisha (2016)*. 86 pp. National Institute of Disaster Management, New Delhi. [https://nidm.gov.in/PDF/pubs/heat\\_wave\\_18.pdf](https://nidm.gov.in/PDF/pubs/heat_wave_18.pdf) (last accessed 01July2022)
- Hoskins, B. J., and D. J. Karoly, 1981: The Steady Linear Response of a Spherical Atmosphere to Thermal and Orographic Forcing. *J. Atmos. Sci.*, **38**, 1179–1196, [https://doi.org/10.1175/1520-0469\(1981\)038<1179:TSLROA>2.0.CO;2](https://doi.org/10.1175/1520-0469(1981)038<1179:TSLROA>2.0.CO;2).
- , and T. Ambrizzi, 1993: Rossby Wave Propagation on a Realistic Longitudinally Varying Flow. *J. Atmos. Sci.*, **50**, 1661–1671, [https://doi.org/10.1175/1520-0469\(1993\)050<1661:RWPOAR>2.0.CO;2](https://doi.org/10.1175/1520-0469(1993)050<1661:RWPOAR>2.0.CO;2).
- Huang, B., C. Liu, V. Banzon, E. Freeman, G. Graham, B. Hankins, T. Smith, and H.-M. Zhang, 2021: Improvements of the Daily Optimum Interpolation Sea Surface Temperature (DOISST) Version 2.1. *J. Clim.*, **34**, 2923–2939, <https://doi.org/10.1175/JCLI-D-20-0166.1>.
- IPCC, 2013: Climate Change 2013: The Physical Science Basis. Contribution of Working Group I to the Fifth Assessment Report of the Intergovernmental Panel on Climate Change [Stocker, T.F., D. Qin, G.-K. Plattner, M. Tignor, S.K. Allen, J. Boschung, A. Nauels, Y. Xia, V. Bex and P.M. Midgley (eds.)]. Cambridge University Press,

Cambridge, United Kingdom and New York, NY, USA, 1535 pp.

IPCC, 2021: Summary for Policymakers. In: *Climate Change 2021: The Physical Science Basis. Contribution of Working Group I to the Sixth Assessment Report of the Intergovernmental Panel on Climate Change* [Masson-Delmotte, V., P. Zhai, A. Pirani, S.L. Connors, C. Péan, S. Berger, N. Caud, Y. Chen, L. Goldfarb, M.I. Gomis, M. Huang, K. Leitzell, E. Lonnoy, J.B.R. Matthews, T.K. Maycock, T. Waterfield, O. Yelekçi, R. Yu, and B. Zhou (eds.)].

Jiménez-Esteve, B., and D. I. V. Domeisen, 2022: The role of atmospheric dynamics and large-scale topography in driving heatwaves. *Q. J. R. Meteorol. Soc.*, **148**, 2344–2367, <https://doi.org/10.1002/qj.4306>.

Jiménez-Esteve, B., K. Kornhuber, and D. I. V. Domeisen, 2022: Heat Extremes Driven by Amplification of Phase-Locked Circumglobal Waves Forced by Topography in an Idealized Atmospheric Model. *Geophys. Res. Lett.*, **49**, e2021GL096337, <https://doi.org/https://doi.org/10.1029/2021GL096337>.

Kalshetti, M., R. Chattopadhyay, K. Hunt, M. K. Phani, S. Joseph, D. Pattanaik, and A. Sahai, 2022: Eddy transport, Wave-mean flow interaction, and Eddy forcing during the 2013 Uttarakhand Extreme Event in the Reanalysis and S2S Retrospective Forecast Data. *Int. J. Climatol.*, <https://doi.org/10.1002/joc.7706>.

Kanamitsu, M., W. Ebisuzaki, J. Woollen, S.-K. Yang, J. J. Hnilo, M. Fiorino, and G. L. Potter, 2002: NCEP–DOE AMIP-II Reanalysis (R-2). *Bull. Am. Meteorol. Soc.*, **83**, 1631–1644, <https://doi.org/10.1175/BAMS-83-11-1631>.

Karoly, D. J., 1983: Rossby wave propagation in a barotropic atmosphere. *Dyn. Atmos. Ocean.*, **7**, 111–125, [https://doi.org/https://doi.org/10.1016/0377-0265\(83\)90013-1](https://doi.org/https://doi.org/10.1016/0377-0265(83)90013-1).

Kenyon, J., and G. C. Hegerl, 2008: Influence of Modes of Climate Variability on Global Temperature Extremes. *J. Clim.*, **21**, 3872–3889, <https://doi.org/https://doi.org/10.1175/2008JCLI2125.1>.

Kornhuber, K., V. Petoukhov, S. Petri, S. Rahmstorf, and D. Coumou, 2017: Evidence for wave resonance as a key mechanism for generating high-amplitude quasi-stationary waves in boreal summer. *Clim. Dyn.*, **49**, 1961–1979, <https://doi.org/10.1007/s00382-016-3399-6>.

- Kornhuber, K., S. Osprey, D. Coumou, S. Petri, V. Petoukhov, S. Rahmstorf, and L. Gray, 2019: Extreme weather events in early summer 2018 connected by a recurrent hemispheric wave-7 pattern. *Environ. Res. Lett.*, **14**, 54002, <https://doi.org/10.1088/1748-9326/ab13bf>.
- , D. Coumou, E. Vogel, C. Lesk, J. F. Donges, J. Lehmann, and R. M. Horton, 2020: Amplified Rossby waves enhance risk of concurrent heatwaves in major breadbasket regions. *Nat. Clim. Chang.*, **10**, 48–53, <https://doi.org/10.1038/s41558-019-0637-z>.
- Lekshmi, S., and R. Chattopadhyay, 2022: Modes of summer temperature intraseasonal oscillations and heatwaves over the Indian region. *Environ. Res. Clim.*, **1**, 025009, <https://doi.org/10.1088/2752-5295/ac9fe7>.
- Lekshmi, S., R. Chattopadhyay, Pai, D.S., 2024 Attribution of Subseasonal Temperature Modes as the Drivers of Dry and Moist Heat Discomfort for the Heat Hazard monitoring over the Indian region, Accepted Manuscript, *Climate Dynamics*, <https://doi.org/10.1007/s00382-024-07236-9>.
- Lin, Q., and J. Yuan, 2022: Linkages between Amplified Quasi-Stationary Waves and Humid Heat Extremes in Northern Hemisphere Midlatitudes. *J. Clim.*, **35**, 8245–8258, <https://doi.org/10.1175/JCLI-D-21-0952.1>.
- Manola, I., F. Selten, H. de Vries, and W. Hazeleger, 2013: “Waveguidability” of idealized jets. *J. Geophys. Res. Atmos.*, **118**, 10,410–432,440, <https://doi.org/https://doi.org/10.1002/jgrd.50758>.
- Matsueda, M., 2011: Predictability of Euro-Russian blocking in summer of 2010. *Geophys. Res. Lett.*, **38**, <https://doi.org/https://doi.org/10.1029/2010GL046557>.
- Mazdiyasni, O., and Coauthors, 2017: Increasing probability of mortality during Indian heat waves. *Sci. Adv.*, **3**, e1700066, <https://doi.org/10.1126/sciadv.1700066>.
- Mearns, L. O., R. W. Katz, and S. H. Schneider, 1984: Extreme High-Temperature Events: Changes in their probabilities with Changes in Mean Temperature. *J. Appl. Meteorol. Climatol.*, **23**, 1601–1613, [https://doi.org/10.1175/1520-0450\(1984\)023<1601:EHTECI>2.0.CO;2](https://doi.org/10.1175/1520-0450(1984)023<1601:EHTECI>2.0.CO;2).
- Meehl, G. A., and C. Tebaldi, 2004: More Intense, More Frequent, and Longer Lasting Heat Waves in the 21st Century. *Science (80-. )*, **305**, 994–997,

<https://doi.org/10.1126/science.1098704>.

Moon, W., B.-M. Kim, G.-H. Yang, and J. S. Wettlaufer, 2022: Wavier jet streams driven by zonally asymmetric surface thermal forcing. *Proc. Natl. Acad. Sci.*, **119**, e2200890119, <https://doi.org/10.1073/pnas.2200890119>.

Murari, K. K., A. S. Sahana, E. Daly, and S. Ghosh, 2016: The influence of the El Niño Southern Oscillation on heat waves in India. **713**, 705–713, <https://doi.org/10.1002/met.1594>.

Pai, D. S., N. SMITHAANIL, and A. N. RAMANATHAN, 2013: Long term climatology and trends of heat waves over India during the recent 50 years (1961-2010). *MAUSAM*, **64**, 585–604, <https://doi.org/10.54302/mausam.v64i4.742>.

———, A. K. Srivastava, and S. A. Nair, 2017: Heat and Cold Waves Over India. *Observed Climate Variability and Change over the Indian Region*, M.N. Rajeevan and S. Nayak, Eds., Springer Singapore, 51–71.

PAI, D. S., and S. NAIR, 2022: Impact of El-Niño-Southern Oscillation (ENSO) on extreme temperature events over India. *MAUSAM*, **73**, 597–606, <https://doi.org/10.54302/mausam.v73i3.5932>.

Parker, T. J., G. J. Berry, and M. J. Reeder, 2014: The Structure and Evolution of Heat Waves in Southeastern Australia. *J. Clim.*, **27**, 5768–5785, <https://doi.org/10.1175/JCLI-D-13-00740.1>.

Perkins-Kirkpatrick, S. E., and S. C. Lewis, 2020: Increasing trends in regional heatwaves. *Nat. Commun.*, **11**, 3357, <https://doi.org/10.1038/s41467-020-16970-7>.

Perkins, S. E., 2015: A review on the scientific understanding of heatwaves-Their measurement, driving mechanisms, and changes at the global scale. *Atmos. Res.*, **164–165**, 242–267, <https://doi.org/10.1016/j.atmosres.2015.05.014>.

Perkins, S. E., L. V Alexander, and J. R. Nairn, 2012: Increasing frequency, intensity and duration of observed global heatwaves and warm spells. *Geophys. Res. Lett.*, **39**, <https://doi.org/https://doi.org/10.1029/2012GL053361>.

Petoukhov, V., S. Rahmstorf, S. Petri, and H. J. Schellnhuber, 2013: Quasiresonant amplification of planetary waves and recent Northern Hemisphere weather extremes. *Proc. Natl. Acad. Sci.*, **110**, 5336–5341, <https://doi.org/10.1073/pnas.1222000110>.

- Rao, V. B., K. K. Rao, B. Mahendranath, T. V Lakshmi Kumar, and D. Govardhan, 2021: Large-scale connection to deadly Indian heatwaves. *Q. J. R. Meteorol. Soc.*, **147**, 1419–1430, <https://doi.org/https://doi.org/10.1002/qj.3985>.
- Ratnam, J. V, S. K. Behera, S. B. Ratna, M. Rajeevan, and T. Yamagata, 2016: Anatomy of Indian heatwaves. *Sci. Rep.*, **6**, 24395, <https://doi.org/10.1038/srep24395>.
- Rohini, P., M. Rajeevan, and A. K. Srivastava, 2016: On the Variability and Increasing Trends of Heat Waves over India. *Sci. Rep.*, **6**, 26153, <https://doi.org/10.1038/srep26153>.
- Roxy, M. K., K. Ritika, P. Terray, R. Murtugudde, K. Ashok, and B. N. Goswami, 2015: Drying of Indian subcontinent by rapid Indian Ocean warming and a weakening land-sea thermal gradient. *Nat. Commun.*, **6**, 7423, <https://doi.org/10.1038/ncomms8423>.
- Seneviratne, S. I., D. Lüthi, M. Litschi, and C. Schär, 2006: Land–atmosphere coupling and climate change in Europe. *Nature*, **443**, 205–209, <https://doi.org/10.1038/nature05095>.
- Shaman, J., and E. Tziperman, 2016: The Superposition of Eastward and Westward Rossby Waves in Response to Localized Forcing. *J. Clim.*, **29**, 7547–7557, <https://doi.org/10.1175/JCLI-D-16-0119.1>.
- Sharma, V. M., G. Pichan, and M. R. Panwar, 1983: Differential effects of hot-humid and hot-dry environments on mental functions. *Int. Arch. Occup. Environ. Health*, **52**, 315–327, <https://doi.org/10.1007/BF02226897>.
- Simmons, A. J., J. M. Wallace, and G. W. Branstator, 1983: Barotropic Wave Propagation and Instability, and Atmospheric Teleconnection Patterns. *J. Atmos. Sci.*, **40**, 1363–1392, [https://doi.org/https://doi.org/10.1175/1520-0469\(1983\)040<1363:BWPAIA>2.0.CO;2](https://doi.org/https://doi.org/10.1175/1520-0469(1983)040<1363:BWPAIA>2.0.CO;2).
- Srivastava, A. K., M. Rajeevan, and S. R. Kshirsagar, 2009: Development of a high resolution daily gridded temperature data set (1969–2005) for the Indian region. *Atmos. Sci. Lett.*, **10**, 249–254, <https://doi.org/https://doi.org/10.1002/asl.232>.
- Taylor, N. A.S., Kondo, N. & Kenney, W. Larry. The physiology of acute heat exposure, with implications for human performance in the heat. In: Taylor, N. A.S. & Groeller, H., editors. *Physiological bases of human performance during work and exercise*. 1 ed. Edinburgh: Elsevier; 2008; 341-358.

- Teng, H., and G. Branstator, 2019: Amplification of Waveguide Teleconnections in the Boreal Summer. **2010**, 421–432.
- White, R. H., K. Kornhuber, O. Martius, and V. Wirth, 2022: From Atmospheric Waves to Heatwaves: A Waveguide Perspective for Understanding and Predicting Concurrent, Persistent, and Extreme Extratropical Weather. *Bull. Am. Meteorol. Soc.*, **103**, E923–E935, <https://doi.org/https://doi.org/10.1175/BAMS-D-21-0170.1>.
- Wolf, G., D. J. Brayshaw, N. P. Klingaman, and A. Czaja, 2018: Quasi-stationary waves and their impact on European weather and extreme events. *Q. J. R. Meteorol. Soc.*, **144**, 2431–2448, <https://doi.org/https://doi.org/10.1002/qj.3310>.